

RESEARCH

Open Access



Development of Mapping Function to Estimate Bond–Slip and Bond Strength of RC Beams Using Genetic Programming

Hoseong Jeong¹ , Seongwoo Ji¹ , Jae Hyun Kim² , Seung-Ho Choi² , Inwook Heo² and Kang Su Kim^{1*}

Abstract

Bond–slip is an important characteristic that determines the stiffness, displacement, and load-bearing capacity of a reinforced concrete (RC) beam. It is essential for performing a precise numerical analysis of the beam. In most cases, bond–slip models can define the bond–slip curve only when there are experimental data. However, many bond test data have been obtained from pull-out tests, and the dominant view is that the bond–slip behavior observed in the pull-out test is quite different from that in an actual RC beam. Therefore, a mapping function that makes it possible to estimate the bond–slip behaviors of beam specimens using those of pull-out specimens was developed in this study. A total of 255 pull-out specimen data and 75 beam specimen data were collected from previous studies, and the importance and influence of each feature of the two groups were analyzed using random forest and K-means clustering. The mapping function was derived using genetic programming, and its accuracy was verified through a comparison with existing models. The proposed model exhibits a high degree of accuracy in estimating bond–slip and bond strength in beam specimens and can provide useful information for understanding the difference in bond–slip behaviors between the two groups.

Keywords: Bond strength, Bond–slip, Mapping, Genetic programming, Beam, Pull-out

1 Introduction

Reinforced concrete (RC) is a composite material composed of concrete and rebar, and the bond between the two materials is a major factor in determining the stiffness, deformation, and load-carrying capacity of RC members (Alharbi et al., 2021; Darwin et al., 1992; Eligehausen et al., 1982; Tefpers, 1979). Therefore, various empirical models to estimate bond strength (τ_{\max}) have been proposed (Esfahani & Kianoush, 2005; Harajli et al., 1995; Orangun et al., 1977; Wu & Zhao, 2013; Xu, 1990). On the other hand, estimation models for bond–slip

($\tau - s$) were very rare (Wu & Zhao, 2013), and bond–slip ($\tau - s$) models presented by most previous research and design codes require experimental data, which makes it difficult to apply them to the numerical analysis of RC members without testing. (Comité Euro-International du Béton, 1993; Eligehausen et al., 1982; Martin, 1973; Mirza & Houde, 1979; Nilson, 1968; Rehm, 1961).

However, the test data available for the derivation of $\tau - s$ are quite limited, and the reason is explained in Fig. 1. The pull-out test is a simple bond testing method by directly pulling out a reinforcing bar embedded in concrete. In this case, tensile stress occurs in the rebar, and compressive stress arises in the surrounding concrete (Alharbi et al., 2021). The other bond test method is the beam test in which a reinforcing bar in an RC beam is pulled out by an external moment. In this case, both the rebar and the surrounding concrete are subjected to tensile stress (Alharbi et al., 2021). Owing to

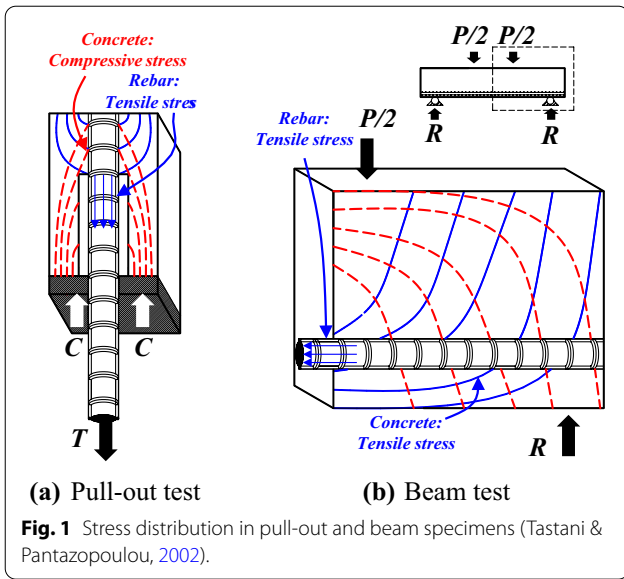
Journal information: ISSN 1976-0485 / eISSN2234-1315.

*Correspondence: kangkim@uos.ac.kr

¹ Department of Architectural Engineering and Smart City Interdisciplinary Major Program, University of Seoul, 163 Seoulsiripdaero, Dongdaemun-gu, Seoul 02504, Republic of Korea
Full list of author information is available at the end of the article



© The Author(s) 2022. **Open Access** This article is licensed under a Creative Commons Attribution 4.0 International License, which permits use, sharing, adaptation, distribution and reproduction in any medium or format, as long as you give appropriate credit to the original author(s) and the source, provide a link to the Creative Commons licence, and indicate if changes were made. The images or other third party material in this article are included in the article's Creative Commons licence, unless indicated otherwise in a credit line to the material. If material is not included in the article's Creative Commons licence and your intended use is not permitted by statutory regulation or exceeds the permitted use, you will need to obtain permission directly from the copyright holder. To view a copy of this licence, visit <http://creativecommons.org/licenses/by/4.0/>.



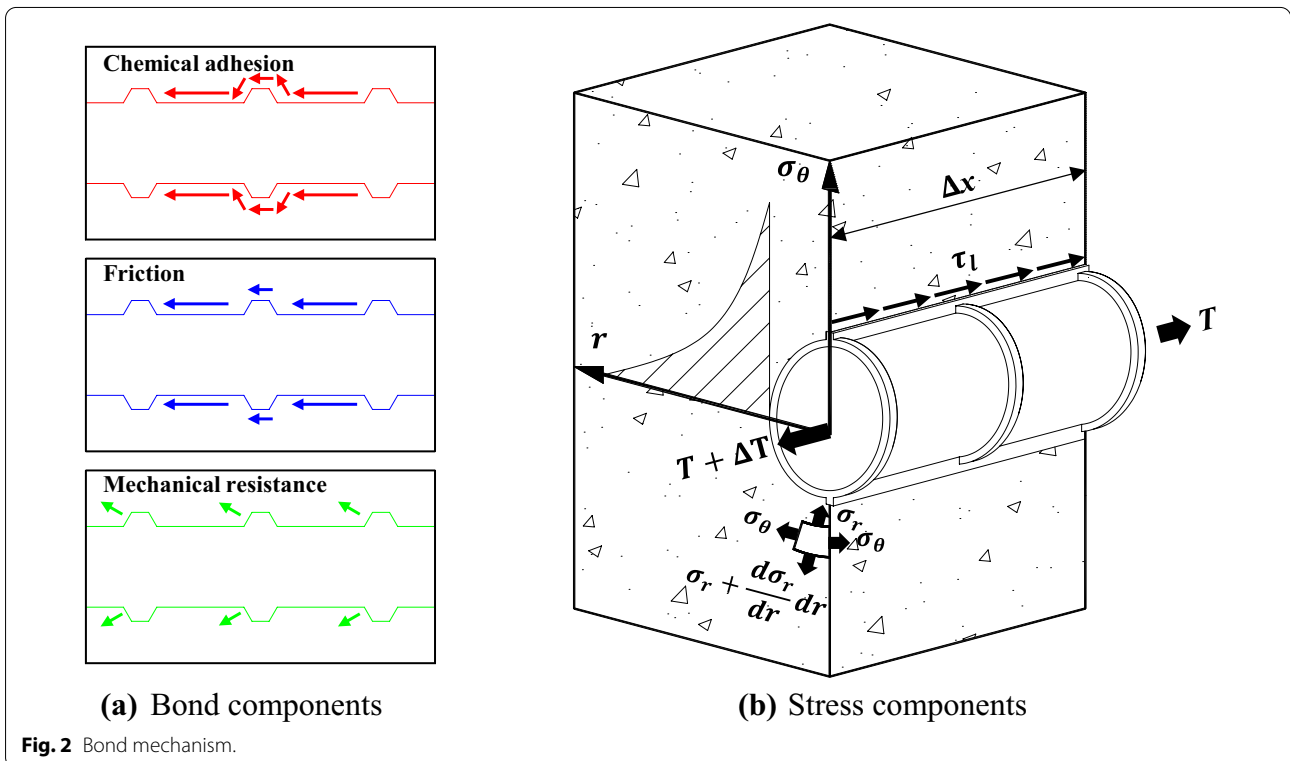
this difference in the stress state, the $\tau - s$ developed in the RC beam may be quite different from the $\tau - s$ obtained from the pull-out specimen (Alharbi et al., 2021). Nevertheless, because of the simplicity of the pull-out test, most of the $\tau - s$ data are pull-out test results, and the beam test data are very limited.

If a mapping function that can convert the $\tau - s$ of pull-out specimens to those of beam specimens is developed, the $\tau - s$ curve of RC beams can be estimated using the large amount of $\tau - s$ data obtained from the pull-out test. Therefore, a mapping function between the $\tau - s$ of pull-out and beam specimens was developed in this study. The overall research process complies with the data science pipeline consisting of data acquisition, analysis, modeling, and verification steps. In the next section, the background and existing models are described. The data and machine-learning methods used in this study are introduced in Sect. 3 and the data analysis results and proposed models are presented in Sect. 4. The verification of the accuracy of the proposed model is described in Sect. 5.

2 Backgrounds

2.1 Bond and stress components

Fig. 2 shows the bond and stress components of the rebar embedded in concrete. As shown in Fig. 2a, the bond components are chemical adhesion, friction, and mechanical interlock (Lutz & Gergely, 1967; Tefers, 1979). Chemical adhesion is a bond component arising from physical and chemical bonding between concrete and rebar and makes little contribution to bond strength, because it disappears when a slip occurs (Alharbi et al., 2021). Friction is caused by the roughness of the surface



and normal stress between the concrete and rebar. Lutz and Gergely reported that normal stress is caused by the shrinkage of concrete (Lutz & Gergely, 1967). Mechanical interlocking is a bond component arising from the shear resistance of the rib and adjacent concrete, which has the greatest effect on the bond strength of the deformed bar (Alharbi et al., 2021; Lutz & Gergely, 1967).

Fig. 2b shows the stress component caused by the bond. The stress that occurs in the longitudinal direction of the rebar is shear stress (τ_l). The average shear stress (τ) caused by the bond is calculated as

$$\tau = \frac{\Delta T}{2\pi d_b \Delta x}, \tag{1}$$

where d_b is the rebar diameter, and ΔT is the increment of the tensile force generated in a unit length (Δx) of rebar. The stress generated in the horizontal direction of the rebar section is divided into radial stress (σ_r) and tangential stress (σ_θ), and the relationship between σ_r and τ is (Tepfers, 1979)

$$\sigma_r = \tau \tan \alpha, \tag{2}$$

where α is the angle between the principal compressive bond stress and the axis of the reinforcing bar, which is approximately 45° (Tepfers, 1979). Based on the thick-wall cylinder theory (Timoshenko, 2002), the tangential stress (σ_θ) can be represented using the following equation:

$$\sigma_\theta = \frac{\left(\frac{d_b}{2}\right)\sigma_r}{\left(c + \frac{d_b}{2}\right)^2 - \left(\frac{d_b}{2}\right)^2} \left[1 + \frac{\left(c + \frac{d_b}{2}\right)^2}{r^2} \right], \tag{3}$$

where c is the cover depth, and r is the radial distance from the center of the rebar. As shown in Eq. (3) and Fig. 2b, σ_θ is maximum at the surface of the reinforcing bar, and it decreases as the r increases.

2.2 Failure Mode, Bond Strength, and Bond–Slip Behavior

Fig. 3 shows the bond–slip curve according to the pull-out failure or splitting failure (Mazumder & Gilbert, 2019). Pull-out failure is a failure mode in which concrete around the rib is crushed. This mainly occurs when the cover depth (c) is great, the compressive strength of concrete (f'_c) is low, or the stress of the concrete near the rib is large, because the embedded length (L_e) is small. Splitting failure is a failure mode in which splitting cracks occur in the longitudinal direction when σ_θ exceeds the tensile strength of concrete (f_t). This mainly occurs when c is shallow or f_t is small. As shown in Fig. 3, splitting failure shows a rapid decrease in bond strength (τ_{max})

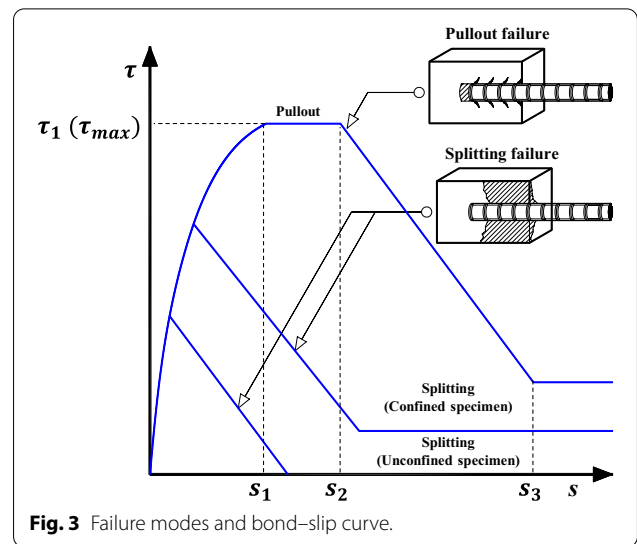


Fig. 3 Failure modes and bond–slip curve.

compared with pull-out failure. There is almost no residual strength in the unconfined specimen, whereas the residual strength is partially maintained in the confined specimen. In addition, the bond strength (τ_{max}) of the confined specimen is larger than that of the unconfined specimen. Therefore, the bond characteristic of rebar varies depending on various influencing parameters and ultimately has a great impact on the behavior of the flexural member.

2.3 Influencing Parameters

Various tests have been conducted on the influencing factors of bonds (Darwin et al., 1992; Eligehausen et al., 1982; Esfahani & Kianoush, 2005; Harajli et al., 1995; Orangun et al., 1977; Soroushian & Choi, 1989; Walker et al., 1997), including f'_c , c , d_b , the cross-sectional area of one leg of transverse reinforcement (A_{st1}), and the spacing of transverse reinforcement (S_{st}). Here, f'_c is the most important influencing factor that increases τ_{max} (Wu & Zhao, 2013), and the effect on τ_{max} is mainly proportional to $\sqrt{f'_c}$ (Esfahani & Kianoush, 2005; Harajli et al., 1995; Orangun et al., 1977). Furthermore, c is an influencing factor that increases τ_{max} , but the effect gradually decreases as c increases (Walker et al., 1997). d_b serves as a factor that decreases τ_{max} and is often reflected in the form of c/d_b (Ichinose et al., 2004). A_{st1} and S_{st} are influencing factors confining longitudinal reinforcing bars, and τ_{max} tends to increase as A_{st1} increases or S_{st} decreases.

2.4 Existing Models

The empirical models to estimate τ_{max} are presented in Table 1. Orangun et al. (1977) proposed an empirical model based on non-linear regression analyses of bond

Table 1 Empirical bond strength models.

Researcher	Equation*
Orangun et al. (1977)	$\tau_{max} = \left(1.2 + \frac{3c}{d_b} + \frac{50d_b}{L_e} + \frac{A_{st1}f_{yt}}{72,500S_{st}d_b}\right)0.083\sqrt{f'_c}$
Xu (1990)	$\tau_{max} = \left(1.6 + \frac{0.7c}{d_b} + 20\rho_{sv}\right)f_t = \left(1.6 + \frac{0.7c}{d_b} + \frac{20A_{st1}}{cS_{st}}\right)f_t$
Harajli et al. (1995)	$\tau_{max} = 0.78\left(\frac{c+K_t}{d_b}\right)^{2/3}\sqrt{f'_c} = 0.78\left[\frac{c+\frac{7A_{st}}{5n}}{d_b}\right]^{2/3}\sqrt{f'_c}$
Esfahani and Kianoush (2005)	$\tau_{max} = \tau_c \frac{1+\frac{1}{M}}{1.85+0.024\sqrt{M}} \left(0.88 + \frac{0.12c_{med}}{c}\right) \left(1 + \frac{0.015A_{st1}A_s}{cS_{st}}\right)$, where $M = \cos h\left(0.0022L_e\sqrt{3\frac{f'_c}{d_b}}\right)$ and $\tau_c = 2.7\frac{\frac{c}{d_b}+0.5}{\frac{c}{d_b}+3.6}\sqrt{f'_c}$
Wu and Zhao (2013)	$\tau_{max} = \frac{2.5\sqrt{f'_c}}{1+3.1e^{-0.47(K_{co}+33K_t)}}$, where $K_{co} = \frac{c}{d_b}$ and $K_t = \frac{A_{st}}{nS_{st}d_b}$

* A_s : cross-sectional area of one longitudinal reinforcement (mm^2), A_{st} : cross-sectional area of all legs of transverse reinforcement (mm^2), A_{st1} : cross-sectional area of one leg of transverse reinforcement (mm^2), L_e : embedded length (mm), S_{st} : spacing of transverse reinforcement (mm), c : minimum of spacing and cover thickness (mm), c_{med} : median of side cover, bottom cover, and rebar spacing, d_b : diameter of rebar (mm), f_t : tensile strength of concrete (MPa), f'_c : compressive strength of concrete (MPa), f_{yt} : yield strength of transverse reinforcement (MPa), n : number of tension bars enclosed by stirrups, s : slip of rebar (mm), τ_{max} : maximum bond stress (MPa).

test data. In this model, the influences of c and f_{yt} (the yield strength of rebar) on the bond strength are reflected linearly. Xu (1990) and Harajli et al. (1995) proposed simpler models, compared to Orangun’s model, where the influence of c is reflected non-linearly and f_{yt} is excluded. Esfahani and Kianoush (2005) proposed an empirical model with high complexity, where the median of side cover, bottom cover, and rebar spacing (c_{med}) is implemented. Wu and Zhao (2013) also proposed a complex bond strength model that provides a unified result with their bond–slip model.

The bond–slip ($\tau - s$) models are shown in Table 2. The top six models require $\tau - s$ test data for completing the curve. On the other hand, Wu and Zhao’s model (2013) gives a complete $\tau - s$ curve without bond test data once the influencing factors, such as compressive strength of concrete (f'_c), cover depth (c), rebar diameter (d_b), cross-sectional area (A_{st}), and spacing of transverse reinforcement (S_{st}), etc., are provided.

3 Materials and Methods

3.1 Materials

As shown in Table 3, 255 and 31 $\tau - s$ data were collected from the previous pull-out and beam tests, respectively. Seven data points were extracted from each $\tau - s$ curve. The data included the points at which slip (s) is the maximum and the minimum, the points at which it is $\tau = \tau_{max}$, and the points which are the closest points to each of 4 points splitting the maximum and the minimum of slip with equal distance. As a result, 1785 and 217 data points were collected from the pull-out and beam test data. The f'_c of pull-out specimens ranged from 5 to 150 MPa, the c from 15 to 96 mm, the d_b from 6 to

Table 2 Empirical bond–slip models.

Researcher	Equation
Rehm (1961)	$\tau = f_{c,cub}(\varphi s^\alpha \pm \psi s)$
Nilson (1968)	$\tau = 998.4s - 58,400s^2 + 852,200s^3$
Martin (1973)	$\tau = \tau_0 + as^b$
Mirza and Houde (1979)	$\tau = 539.8s - 25,610s^2 + 592,200s^3 - 5,574,000s^4$
Eligehausen et al. (1982)	$\tau = \tau_{max}\left(\frac{s}{s_1}\right)^\alpha$, where $0 \leq s \leq s_1$
Comité Euro-International du Béton (1993)	$\tau = \tau_{max}$, when $s_1 < s \leq s_2$ $\tau = \tau_{max} - (\tau_{max} - \tau_f)\frac{s-s_2}{s_3-s_2}$, when $s_2 < s \leq s_3$ $\tau = \tau_f$, when $s_3 < s$
Wu and Zhao (2013)	$\tau = \frac{\tau_{max}}{\left[\frac{e^{-B} \ln(B/D)/(B-D)}{e^{-D} \ln(B/D)/(B-D)}\right]}(e^{Bs} - e^{Ds})$, where $B = \frac{0.0254+K_t}{-0.0232-8.34K_t}$, $D = 3\ln\left(\frac{0.7315+K}{5.176+0.3333K} - 0.13\right) - 3.375$ and $K = K_{co} + 7K_t$

* $K_{co} = \frac{c}{d_b}$, $K_t = \frac{A_{st}}{nS_{st}d_b}$, a : experimental constant, b : experimental constant, $f_{c,cub}$: compressive strength of cubic concrete (MPa), s : slip of rebar (mm), s_1 : initial slip in bond–slip model related to peak stress (mm), s_2 : end slip in bond–slip model related to peak stress (mm), s_3 : slip in bond–slip model related to residual stress (mm), s_4 : slip at 0 bond stress (mm), α : theoretical or experimental constant (MPa), τ : bond stress (MPa), τ_0 : adhesive bond stress (MPa), τ_f : residual bond stress (MPa), φ : theoretical or experimental constant, ψ : theoretical or experimental constant.

32 mm, the A_{st1}/S_{st} from 0 to 3.6, the s from 0 to 25 mm, and the τ from 0 to 48 MPa. Similarly, the f'_c of the beam specimens ranged from 24 to 93 MPa, the c from 15 to 59 mm, the d_b from 8 to 40 mm, the A_{st1}/S_{st} from 0 to 2, the s from 0 to 4.2 mm, and the τ from 0 to 28 MPa. In addition, as shown at the bottom of Table 3, 44 beam test data with only τ_{max} reported were collected to compensate for the lack of data in the beam test. The f'_c of the data ranged from 29 to 93 MPa, the c from 15 to 76 mm,

Table 3 Summary of data.

$\tau - s$ data (Pull-out specimens)										
Researchers	S	N_s (EA)	N (EA)	f'_c (MPa)	c (mm)	d_b (mm)	c/d_b	A_{st1}/S_{st}	s (mm)	τ (MPa)
Baena et al., (2009)	P	2	14	27	92–94	12–16	5.8–7.8	0	0–25	0–13
Campione et al., (2004)	P	4	28	34	36	12	3	0–0.9	0–12.1	0–16
Eligehausen et al., (1982)	P	8	56	29–32	57–96	19–32	3	0–3.6	0–12.1	0–16
Engstrom et al., (1998)	P	3	21	28–29	16	16	1	0–0.4	0–15	0–8
Harajli et al., (1995)	P	2	14	22	60–80	20–25	3–3.2	0.9–1.1	0–18.1	0–13
Kim et al., (2015)	P	2	14	29–33	75	16	4.7	0	0–4.6	0–25
Lee et al., (2012)	P	5	35	26–42	45	13	3.4	0	0–10	0–18
Liu et al., (2020)	P	5	35	38–82	90–94	12–20	4.5–7.8	0	0–12	0–32
Ma et al., (2017)	P	3	21	25	30–66	18–22	1.4–3.7	0	0–1.5	0–8
Melo et al., (2015)	P	1	7	16	94	12	7.8	0	0–10	0–13
Mo and Chan (1996)	P	1	7	27	66–69	13	5.1–5.3	0	0–1.1	0–9
John Robert Prince and Singh (2013)	P	6	42	20–37	38–94	12–25	1.5–7.8	0	0–15.3	0–18
Solyom and Balázs (2020)	P	6	42	35	47–72	6–8	7.8–12	0	0–10	0–15
Song et al., (2015)	P	48	336	8–53	15–67	14–16	1.1–4.2	0–0.3	0–16.1	0–25
Soroushian and Choi (1989)	P	5	35	30–32	48–96	16–32	3	0.8–1.5	0–12.1	0–17
Soroushian et al., (1991)	P	8	56	24–54	75–96	25–32	3	0–1	0–12.7	0–20
Sturm and Visintin (2019)	P	3	21	150	20–75	16	1.3–4.7	0	0–2	0–48
Wu et al., (2021)	P	132	924	5–48	64–69	12–22	2.9–5.8	0	0–14.2	0–22
Yalciner et al., (2012)	P	6	42	23–51	15–45	14	1.1–3.2	0	0–11.9	0–27
Zhou et al., (2015)	P	1	7	18	91	18	5.1	1.3	0–10	0–5
de Almeida Filho et al., (2008)	P	4	28	32–50	45–72	10–16	4.5	0	0–6.3	0–22
Total (or min–max)		255	1,785	5–150	15–96	6–32	1–5.8	0–3.6	0–25	0–48
$\tau - s$ data (Beam specimens)										
Desnerck et al., (2010)	B	5	35	64	38–59	12–40	1.4–3.7	0.6–1.6	0–2	0–28
Hou et al., (2020)	B	3	21	39	30	16	2	0–0.4	0–2.2	0–13
Robert and David (1961)	B	10	70	24–31	38–44	13–25	1.5–3.4	1	0–0.8	0–11
Petean et al., (2013)	B	4	28	50–51	41–42	16–18	2.3–2.6	1.7–2	0–4	0–25
Seis and Beyciođlu (2017)	B	3	21	38	44–46	8–12	3.7–5.8	1	0–0.7	0–8
Yerlici and Ozturan (2000)	BE	4	28	71–93	15	12–16	0.9–1.3	0	0–0.3	0–14
de Almeida Filho et al., (2008)	B	2	14	30	42–45	10–16	2.6–4.5	0.6–1.6	0–4.2	0–12
Total (or min–max)		31	217	24–93	15–59	8–40	0.9–5.8	0–2	0–4.2	0–28
τ_{max} data only (Beam specimens)										
Lin and Zhao (2016)	B	6	6	30	40	20	2.0	0.8–1.6	–	8–9
Kemp and Wilhelm (1979)	BE	6	6	29–30	25–76	16	1.6–4.8	0–0.8	–	4–7
Yerlici and Ozturan (2000)	BE	32	32	64–93	15–30	12–26	0.6–1.9	0–0.9	–	9–18
Total (or min–max)		44	44	29–93	15–76	12–26	0.6–4.8	0–1.6	–	4–18

A_{st1} : cross-sectional area of transverse reinforcement (one leg, mm^2), L_e : embedded length (mm), N : number of data points (EA), N_s : number of specimens (EA), S : type of specimens (P: Pull-out, B: Beam, BE: Beam end), S_{st} : spacing of transverse reinforcement (mm), c : minimum value among bottom cover, side cover, and spacing (mm), d_b : diameter of rebar (mm), f'_c : compressive strength of concrete (MPa), s : slip (mm), τ : bond stress (MPa).

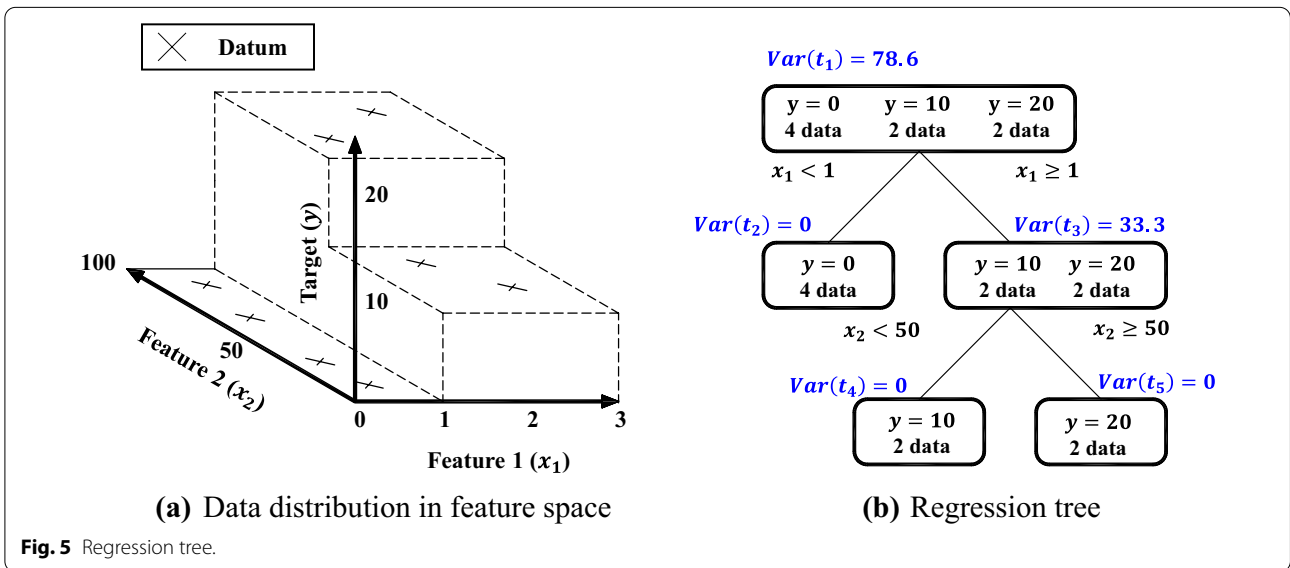
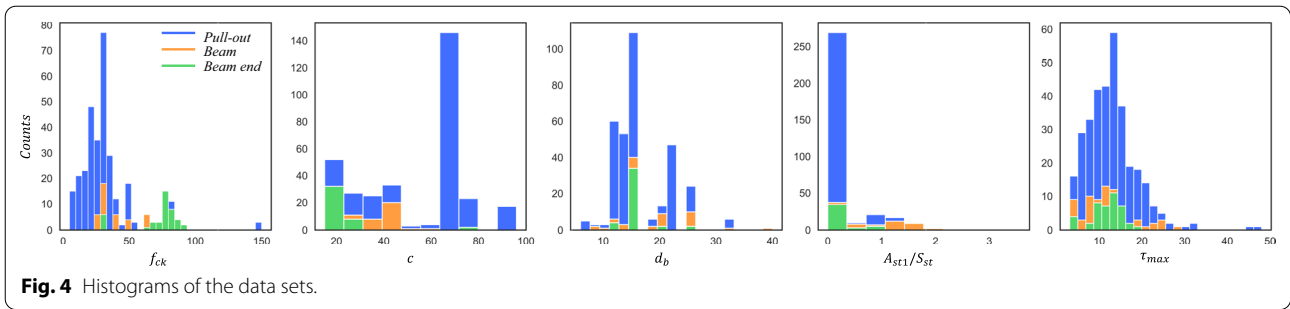
Specimens that $\tau_{max}\pi d_b L_e \geq A_s f_y$ were excluded from data sets.

the d_b from 12 to 26 mm, the A_{st1}/S_{st} from 0 to 1.6, and the τ from 4 to 18 MPa. Fig. 4 shows the histograms of τ_{max} data. The features and counts are presented in x - and y -axes, respectively. The highest frequency occurred at $f_{ck} = 30$ MPa, $c = 67$ mm, $d_b = 16$ mm, $A_{st1}/S_{st} = 0$ mm, and $\tau_{max} = 13$ MPa.

3.2 Methods

3.2.1 Random Forest

A regression tree (RT) (Breiman et al., 1984) can be used advantageously in modeling and data analysis, because it can provide a regression model with moderate accuracy and feature importance. Fig. 5a shows the regression



model of data consisting of two features ($x_{1,i}, x_{2,i} \in X$) and a target ($y_i \in Y$) to explain the learning process of RT. As shown in Fig. 5b, the learning process of an RT is to build up splits (s_p , i.e., if-else function) that can minimize the impurity (I) of data from the root node.

The first step in the learning process is to define the impurity (I), and the I that a node t has in a regression problem can be defined as variance ($\text{Var}(t)$), as follows:

$$I(t) = \text{Var}(t) = \frac{1}{N(t)} \sum_{x_i \in t} (y_i - \bar{y}(t))^2, \quad (4)$$

where $N(t)$ is the number of data in node t , and $\bar{y}(t)$ is the average of y in node t . The next step is to define a split set ($S_p, s_p \in S_p$), which is created by sorting the values of each feature in order and adopting the mid-point. For example, when the x_1 of the data included in t are 0.5, 1.5, and 2.5 and the x_2 are 20, 40, 60, and 80, $S_p = \{(x_1 : 1), (x_1 : 2), (x_2 : 30), (x_2 : 50), (x_2 : 70)\}$. The next step is to derive the $s_{p,\max} \in S_p$ that can minimize the impurity change (ΔI), and ΔI can be calculated as

$$\Delta I(s_p, t) = I(t) - I(t_L) - I(t_R), \quad (5)$$

where t_L and t_R are the left and right child nodes generated from s_p , respectively. For each s_p , ΔI is calculated, and $s_{p,\max}$ is derived based on the $\arg \max_{s_p \in S_p} \Delta I$ value.

Through the repetition of the above process, an RT is built, and the feature importance is derived based on the ΔI .

The RT is prone to overfitting, because it can build a regression model that fits the training set perfectly. In addition, because the RT selects s_p based on variance, it is greatly affected by the data distribution. One method devised to compensate for these problems is the random forest (RF) (Breiman, 2001), and the main concept of this method is the bagging and random selection of features. Bagging is a method of creating multiple trees using various data sets generated through sampling with replacements and averaging the predicted values of all trees to determine the final predicted value. The random selection of features is a method of limiting the number of

features that can be used to generate S_p , and it serves to decorrelate the trees that make up the RF. The regression model derived from this method exhibits superior generalization performance to that of the RT (Breiman, 2001).

3.2.2 K-Means Clustering

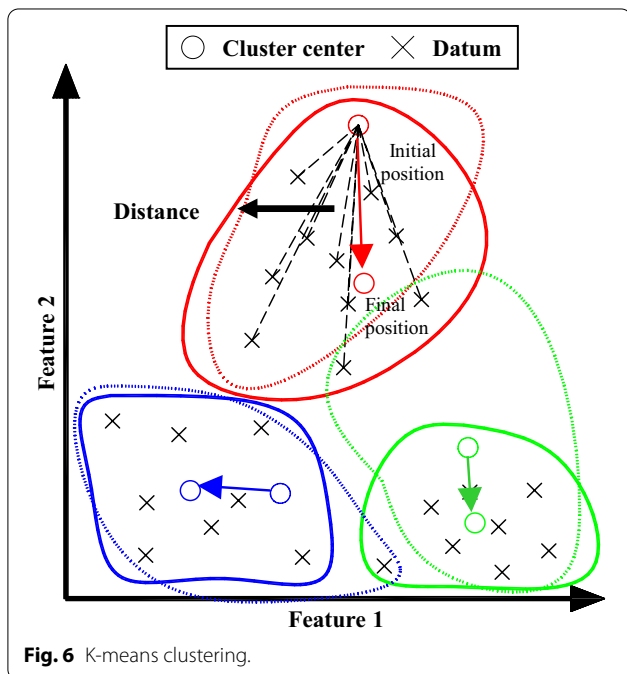
Clustering is the task of grouping similar data and is useful in data mining, because it can summarize data (Xu & Wunsch, 2008). K-means clustering, one of the most common methods used in clustering, is an algorithm that groups a given data set into a set of K clusters (Ding & He, 2004). Fig. 6 shows the process of K-means clustering, where \times is each datum, and o is the center of the cluster. The dotted line represents the distance (D) between a cluster center and a datum, and the Euclidean distance (L_2) can be used to measure D , as shown below:

$$D(x_1, x_2) = (|x - \mu|^{\frac{1}{2}})^2, \tag{6}$$

where x is the datum, and μ is the center of the cluster. The objective of K-means clustering is to minimize the variance between μ and x of each cluster, which can be represented as

$$\operatorname{argmin}_C \sum_{i=1}^k \sum_{x \in C_i} (x - \mu_i)^2 \tag{7}$$

To do this, the algorithm repeats the following process.

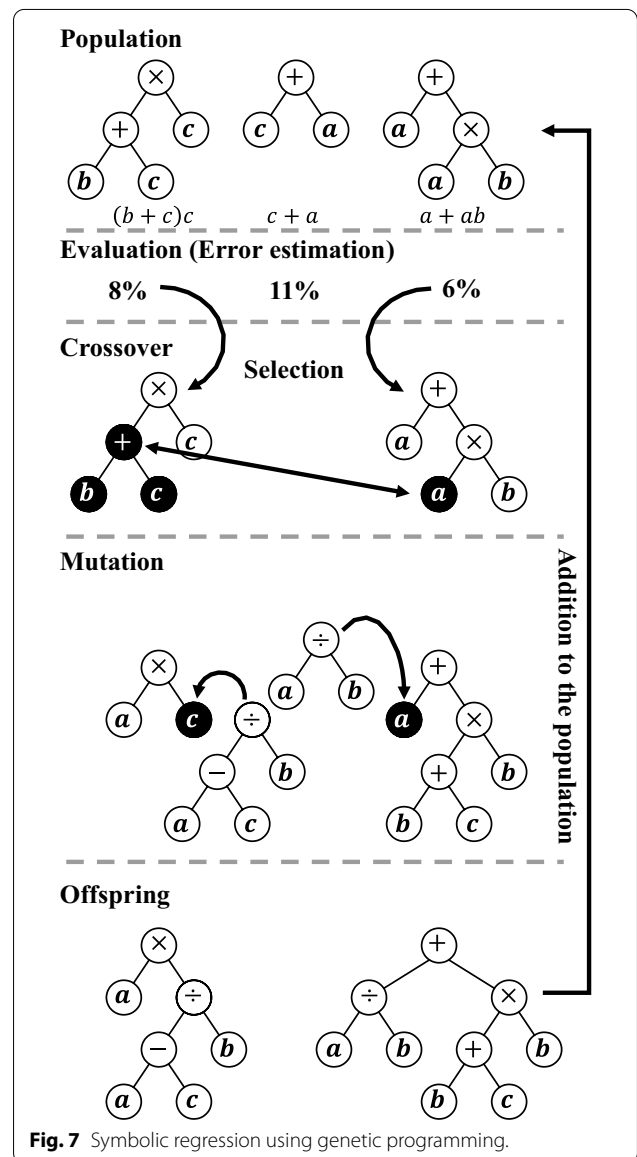


1. Determine which cluster the data belong to: Identify the D between x and μ and then determine the cluster to which each x belongs based on Eq. (7).
2. Move the centroid of the cluster: Move μ to the centroid of each cluster.

The process continues until the centroid of the cluster no longer changes.

3.2.3 Genetic Programming

Genetic programming (GP) is an optimization algorithm that simulates evolution and can be used for symbolic regression, classification, and feature selection (Koza, 1994). Fig. 7 shows the symbolic regression using GP.



The algorithm creates several expression trees (a formula expressed as a tree type) to generate a population. Subsequently, it evaluates the fitness (f , i.e., estimation error) of each tree, where the mean squared error (MSE) or mean absolute error (MAE) can be used to calculate f based on true (y_i) and prediction values (y_{pi}):

$$MSE(y_i - y_{pi}) = \frac{1}{N} \sum_{i=1}^N (y_i - y_{pi})^2. \tag{8}$$

$$MAE(y_i - y_{pi}) = \frac{1}{N} \sum_{i=1}^N |y_i - y_{pi}|. \tag{9}$$

Based on the previously evaluated f , two excellent parent trees are selected to perform a crossover that exchanges a part of each tree. Subsequently, a mutation is carried out to change a part of the tree to a random tree. The generated offspring tree is merged into the next-generation population, and this process continues until a user-defined termination condition is met.

4 Results and Discussion

4.1 Parametric Study

4.1.1 Feature Importance

There are some machine learning-based methods to analyze the feature importance of the data set (Kuhn & Johnson, 2019). For example, recursive feature elimination (RFE), which observes the change of the model performance by recursively eliminating a variable in the training data set, can be used for deriving feature importance. However, RFE can underestimate the importance of the features with colinearity (Granitto et al., 2006).

Meanwhile, although impurity-based feature importance, such as RF tends to underestimate the importance of categorical features, it is less affected by collinearity than RFE (Deng et al., 2011). In this paper, there was no categorical feature in the data sets, but there was collinearity between some features. Thus, the feature importance of τ_{max} was analyzed using the RF introduced in Sect. 3.2.1. To confirm the difference in the feature importance of the pull-out and beam specimens, two data sets were trained separately, and the ratio of training data to test data was 2:1. Hyperparameter optimization was performed to derive the feature importance from the optimized RF model. For the pull-out data, the lowest test error occurred when the number of trees was 100, the depth of the tree was 20, and the maximum number of features was 3. The optimal result was obtained when they were 1000, 10, and 4, respectively, for the beam data set.

Fig. 8a, b shows the feature importance results of the pull-out and beam specimens derived by RF, respectively. As shown in Fig. 8a, f'_c had a significant influence on the bond strength of the pull-out specimens ($\tau_{p,max}$). The level of importance was the highest in f'_c , followed by c , d_b , and $\frac{A_{st1}}{S_{st}}$. However, the degree of influence of f'_c on the bond strength of the beam specimens ($\tau_{b,max}$) was reduced compared with that of $\tau_{p,max}$, and the influence of $\frac{A_{st1}}{S_{st}}$ increased significantly. As a result, the level of importance was the highest in f'_c , followed by $\frac{A_{st1}}{S_{st}}$, c , and d_b , for the bond strength of the beam specimens ($\tau_{b,max}$).

4.1.2 Correlation Analysis

The correlation between the features and τ_{max} was analyzed in this section. To identify the correlation between a target and a selected feature more clearly, the influence of other features should be minimized. Thus, K-mean

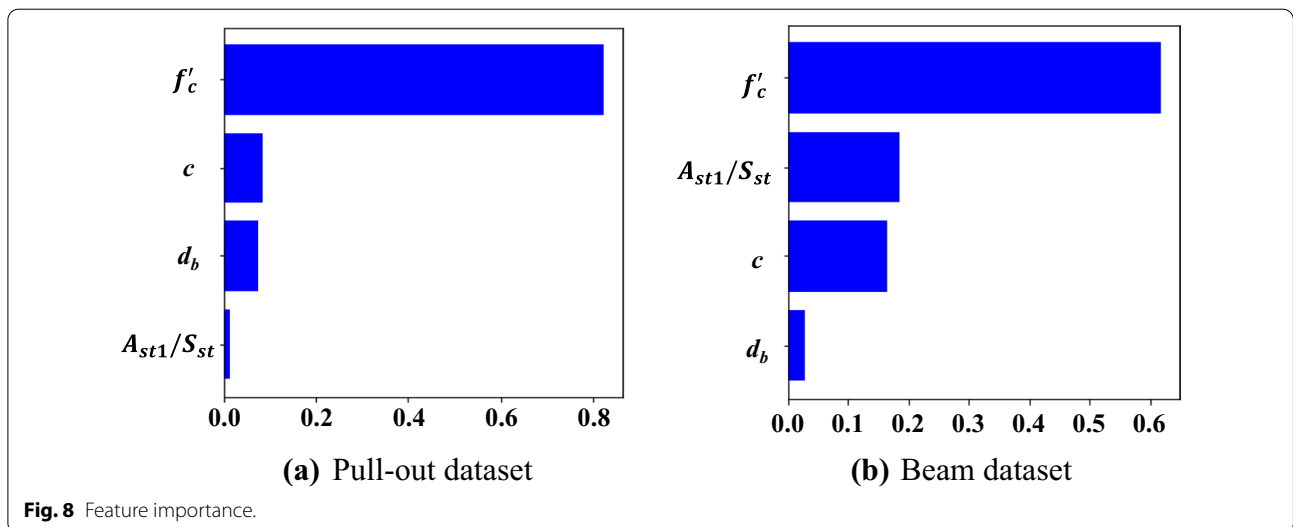


Fig. 8 Feature importance.

clustering, the distance-based clustering method introduced in Sect. 3.2.2, was used to cluster the data that are close to each other. The number of clusters was selected based on the silhouette coefficient (Rousseeuw, 1987),

and the highest silhouette coefficient was obtained from four and three clusters, respectively, for the pull-out and beam specimens.

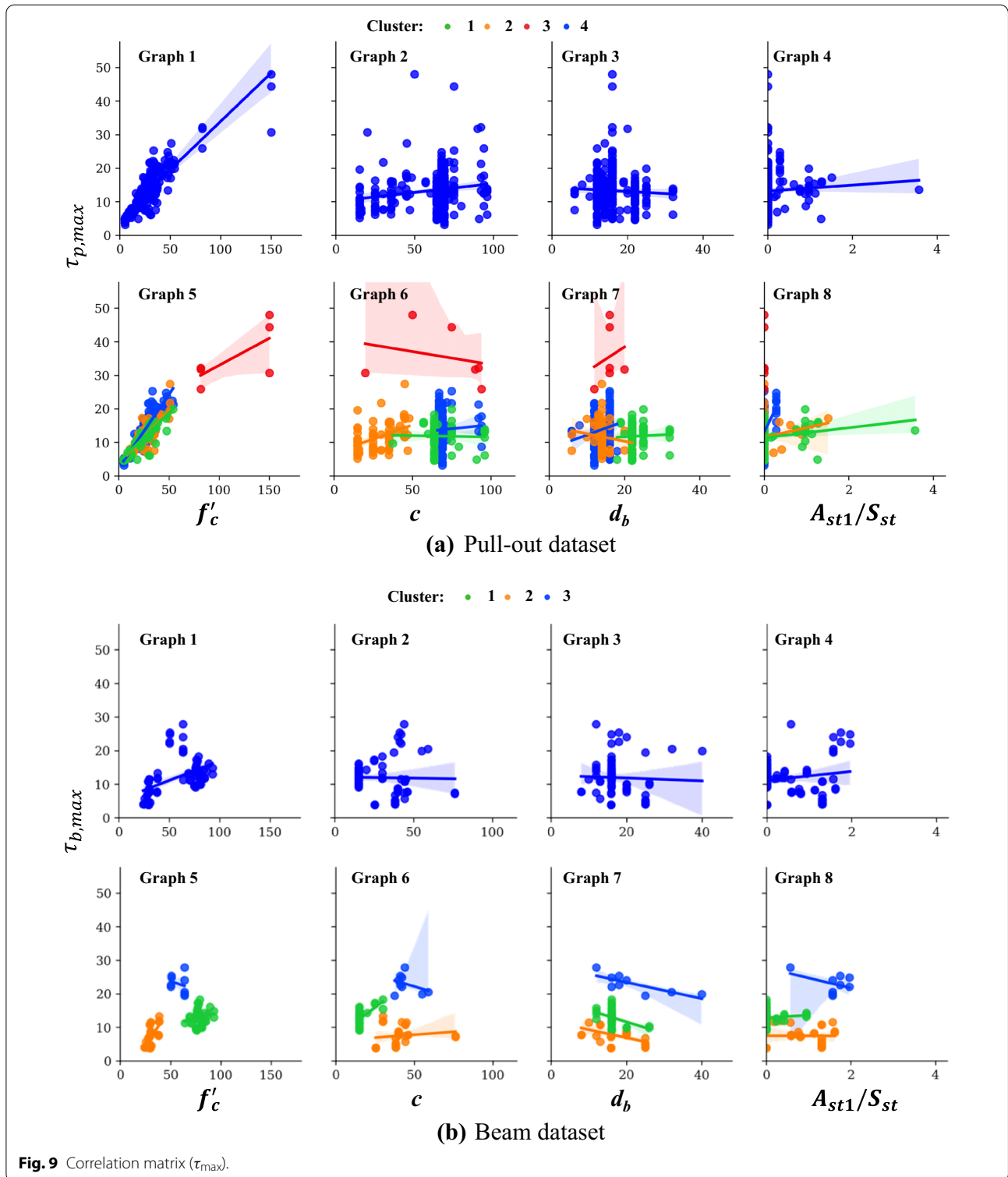


Fig. 9a, b shows the results of the correlation analysis between the target and the features constituting the pull-out and beam specimens. The x -axis of each graph represents the features shown at the bottom, and the y -axis represents τ_{max} . The scatter plot and linear regression model of the unclustered data and clustered data are shown at the top and bottom of the figure, respectively. The graphs are numbered in the upper-left corner of each graph.

As shown in Fig. 9a Graph 1, the variable with the greatest slope in the pull-out specimens was f'_c , and the effect of f'_c decreased slightly with increasing f'_c , as shown in Graph 5. As c , which showed the second-highest feature importance, increased, $\tau_{p,max}$ increased (Graph 2), and the increase in $\tau_{p,max}$ gradually decreased as c increased (Graph 6). In addition, d_b showed different tendencies for each cluster (Graph 7), but $\tau_{p,max}$ decreased slightly as d_b increased for unclustered data (Graph 3). Moreover, A_{st1}/S_{st} slightly increased $\tau_{p,max}$ (Graph 4), and a consistent tendency was found in all clusters (Graph 8).

In the beam specimens, f'_c increased $\tau_{b,max}$ as in pull-out specimens, but the increase was smaller than that of the pull-out specimens (Fig. 9b Graph 1). The influence of c , which showed the third-highest degree of influence, was obscure (Graph 2 and 6). Unlike the pull-out

specimens in which d_b had the lowest degree of influence, d_b showed a distinct influence to decrease $\tau_{b,max}$ (Graph 7). Finally, A_{st1}/S_{st} , which showed the second-largest feature importance, was found to increase $\tau_{b,max}$ (Graph 4).

Tables 4 and 5 show the average feature values of each cluster obtained from the pull-out and beam specimens, respectively. As shown in Table 4, clusters 2 and 3 with underlines showed the lowest and highest $\tau_{p,max}$, respectively, and there were significant differences in f'_c and c/d_b . It can be confirmed that the effect of f'_c was much larger than that of c/d_b , when comparing the differences in clusters 2, 3, and 4. In the beam specimens, clusters 2 and 3 with underlines in Table 5 showed the lowest and highest $\tau_{max,b}$, respectively, and major differences occurred in f'_c and A_{st1}/S_{st} . Although cluster 1 had the highest f'_c , the cluster with the highest $\tau_{b,max}$ was cluster 3 which has the second-best f'_c and first-best A_{st1}/S_{st} . This is because the influence of f'_c decreased and because the influence of A_{st1}/S_{st} increased in the beam specimens, as shown in Figs. 8b and 9b.

4.2 Derivation of Mapping Function

4.2.1 Evolutionary Parameter

In this section, the mapping function ($\tau - s$ relationship between pull-out and beam specimens) was modeled

Table 4 Feature values of each cluster (pull-out data set).

Pull-out						
Cluster	f'_c (MPa)	c (mm)	d_b (mm)	c/d_b	A_{st1}/S_{st}	$\tau_{p,max}$ (MPa)
1	26	68	23	2.9	0.3	12
2	<u>26</u>	29	14	<u>2.1</u>	<u>0.1</u>	<u>12</u>
3	<u>116</u>	70	16	<u>4.4</u>	<u>0.0</u>	<u>36</u>
4	26	70	14	5.0	0.0	14

The feature values are presented as the mean within the cluster

Underlined values indicate the feature values of clusters with the highest and lowest $\tau_{p,max}$

A_{st1} : cross-sectional area of one leg of transverse reinforcement (mm^2), S_{st} : spacing of transverse reinforcement (mm), c : compressive strength of concrete (MPa), d_b : diameter of rebar (mm), f'_c : compressive strength of concrete (MPa), $\tau_{p,max}$ maximum bond stress of a pullout specimen (MPa)

Table 5 Feature values of each cluster (beam data set).

Beam						
Cluster	f'_c (MPa)	c (mm)	d_b (mm)	c/d_b	A_{st1}/S_{st}	$\tau_{b,max}$ (MPa)
1	79	17	16	1.0	0.1	13
2	<u>31</u>	40	18	<u>2.3</u>	<u>0.9</u>	<u>7</u>
3	<u>58</u>	45	22	<u>2.0</u>	<u>1.6</u>	<u>23</u>

The feature values are presented as the mean within the cluster

Underlined values indicate the feature values of clusters with the highest and lowest $\tau_{b,max}$

A_{st1} : cross-sectional area of one leg of transverse reinforcement (mm^2), S_{st} : spacing of transverse reinforcement (mm), f'_c : compressive strength of concrete (MPa), d_b : diameter of rebar (mm), f'_c : compressive strength of concrete (MPa), $\tau_{b,max}$ maximum bond stress of a pullout specimen (MPa)

Table 6 Evolutionary parameters.

Parameter		$\tau_p - s$ relationship (Bond slip of pull-out data set)	$\tau_p - \tau_b$ relationship (Mapping function)
Instruction		$f'_c, c, d_b, A_{st1}/S_{st}, s,$ $+, -, \times, \div$	$f'_c, c, d_b, A_{st1}/S_{st}, \tau_p,$ $+, -, \times, \div$
Initialization	Method	Ramped half and half	
	Depth	1 ~ 4	
	Ratio	50%	
Population size		1000	100,000
Selection	Method	Tournament selection	
	Size	7	
Crossover rate	Probability	90%	
	Max. size	40	30
Mutation rate	Probability	10%	
	Max. size	40	30
	Depth of mutation trees	0 ~ 2	
Generation		250	50

* τ_p : Bond-slip function for pull-out specimens.

based on data, and the GP introduced in Sect. 3.2.3 was used to do this. Before deriving the mapping function, a generalized $\tau - s$ model ($\tau_p(s)$) of the pull-out specimen was derived. The evolutionary parameters used in the GP are summarized in Table 6. The instructions used to model $\tau_p(s)$ were $f'_c, c, d_b, \frac{A_{st1}}{S_{st}}, s$, and arithmetic operators (i.e., $+, -, \div, \times$). Since the mapping function between the bond-slip model of the beam specimens (τ_b) and τ_p is

$$\tau_b = m(\tau_p, f'_c, c, d_b, A_{st1}/S_{st}), \tag{10}$$

$\tau_p, f'_c, c, d_b, \frac{A_{st1}}{S_{st}}$, and the arithmetic operators were used as instructions. The ramped half-and-half (Koza, 1994) method was used to generate the initial population, and the size of the tree was set at 1 to 4. Because a larger training data set requires a higher computational cost for evaluation, the population size was set to 1000 in the τ_p modeling, while it was set to 100,000 in the modeling of $m(\tau_p)$. Tournament selection (Miller & Goldberg, 1995) was used as a selection method, and the tournament size was set to 7. The crossover and mutation probabilities were set to 90% and 10%, respectively, and the maximum size of the tree was set to 40 and 30, respectively, for $\tau_p(s)$ and $m(\tau_p)$ modeling to derive a concise equation. In $\tau_p(s)$ modeling, the MAE of the GP did not decrease significantly after approximately 250 generations, and the algorithm was thus terminated in the 250th generation. Even in $m(\tau_p)$ modeling, the algorithm was terminated in the 50th generation for the same reason. As with the RF, the ratio of the training and test data was 2:1.

4.2.2 Bond-Slip and Bond Strength Model for Pull-Out Specimens

The $\tau_p(s)$ obtained using GP is shown below.:

$$\tau_p = \frac{2\left(f'_c + \frac{155}{f'_c} + \frac{155}{c} + 45\right)s}{2s^2 + \left(\frac{155}{f'_c} + \frac{310}{c}\right)s + 1} \tag{11}$$

To simplify Eq. (11), $\left(\frac{155}{f'_c} + \frac{310}{c}\right)s$ is removed from the denominator of Eq. (11), and constant optimization is performed using the Levenberg–Marquardt (Levenberg, 1944; Marquardt, 1963) algorithm. The modified $\tau_p(s)$ is expressed as

$$\tau_p = \left(f'_c - \frac{130}{f'_c} - \frac{630}{c} + 50\right) \frac{s}{2(s^2 + 1)}. \tag{12}$$

In Eq. (12), f'_c is modeled in the form of $f'_c - \frac{\alpha}{f'_c}$ (where α is a constant), which is a combination of a rational function and a linear function. This is the result of reflecting the effect that the increase in bond strength decreased with increasing f'_c , as shown in Fig. 9a Graph 5. In addition, c appears in the form of $-\frac{\alpha}{c}$ (where α is a constant), which is a result of reflecting the decrease of influence on τ_p as c increase. However, d_b , and A_{st1}/S_{st} are not reflected in Eqs. (11) and (12). This is because their feature importance is low, as shown in Fig. 8a, and their influence on bond strength is relatively low, as shown in Fig. 9a. τ_p is differentiated with respect to s to derive the bond strength of the pull-out specimens ($\tau_{p,max}$) from Eq. (12). The $d\tau_p/ds$ is

$$\frac{d\tau_p}{ds} = \left(f'_c - \frac{130}{f'_c} - \frac{630}{c} + 50 \right) \frac{(-s^2 + 1)}{2(s^2 + 1)^2}. \quad (13)$$

Equation 13 confirms that a maximum point is obtained at $s = 1$. $s = 1$ is substituted into Eq. (12) to obtain the bond strength of the pull-out specimens ($\tau_{p,max}$). The $\tau_{p,max}$ is

$$\tau_{p,max} = \frac{1}{4} \left(f'_c - \frac{130}{f'_c} - \frac{630}{c} + 50 \right). \quad (14)$$

4.2.3 Mapping Function Between Pull-Out and Beam Bond-Slip Data

The $m(\tau_p)$ derived using GP is

$$\tau_b = m(\tau_p) = \frac{(A_{st1}/S_{st} + 1)f'_c + 14}{d_b + 7\tau_p} \tau_p + \frac{c}{d_b + 7\tau_p}. \quad (15)$$

Unlike in Eq. (11), the effects of d_b and A_{st1}/S_{st} are reflected in Eq. (15). This is because, as shown in Fig. 9b, their influence increase in the beam tests. Meanwhile, in Eq. (15), τ_b is not equal zero at $s = 0$ because of the $\frac{c}{d_b + 7\tau_p}$ term. Accordingly, the $\frac{c}{d_b + 7\tau_p}$ term is removed from Eq. (15), and the influence of c is then reflected in the denominator of d_b to introduce c/d_b , a term used widely in the τ_{max} prediction model. In addition, a constant term is added to the denominator to build a model with a higher

level of accuracy, and constant optimization is performed. The modified $m(\tau_p)$ is

$$\tau_b = m(\tau_p) = \frac{(A_{st1}/S_{st} + 2.7)f'_c - 16}{210\frac{d_b}{c} + 7\tau_p - 10} \tau_p. \quad (16)$$

In Eq. (16), the influence of A_{st1}/S_{st} is reflected linearly, and d_b is reflected in the form of a rational function that gradually reduce τ_b . τ_b is differentiated with respect to s to derive the bond strength of the beam specimens ($\tau_{b,max}$) from Eq. (16) as below:

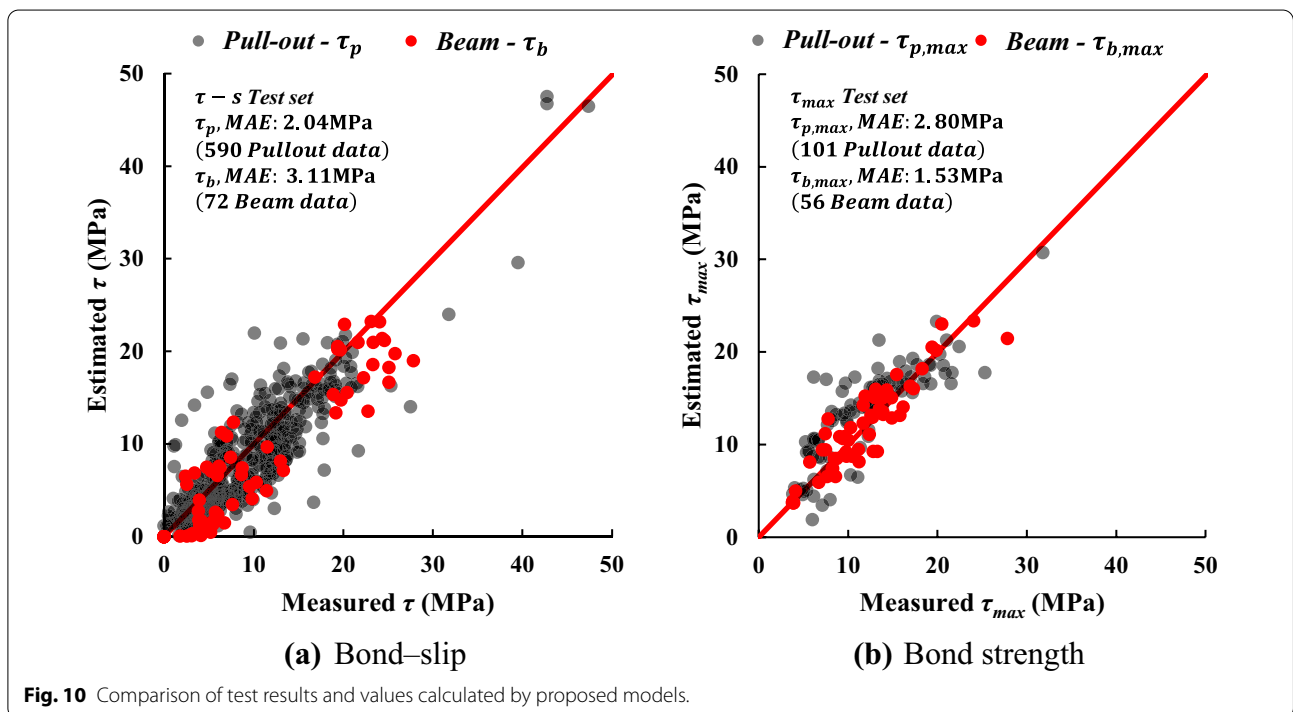
$$\tau_b = \frac{dm}{ds} = \frac{dm}{d\tau_p} \frac{d\tau_p}{ds}. \quad (17)$$

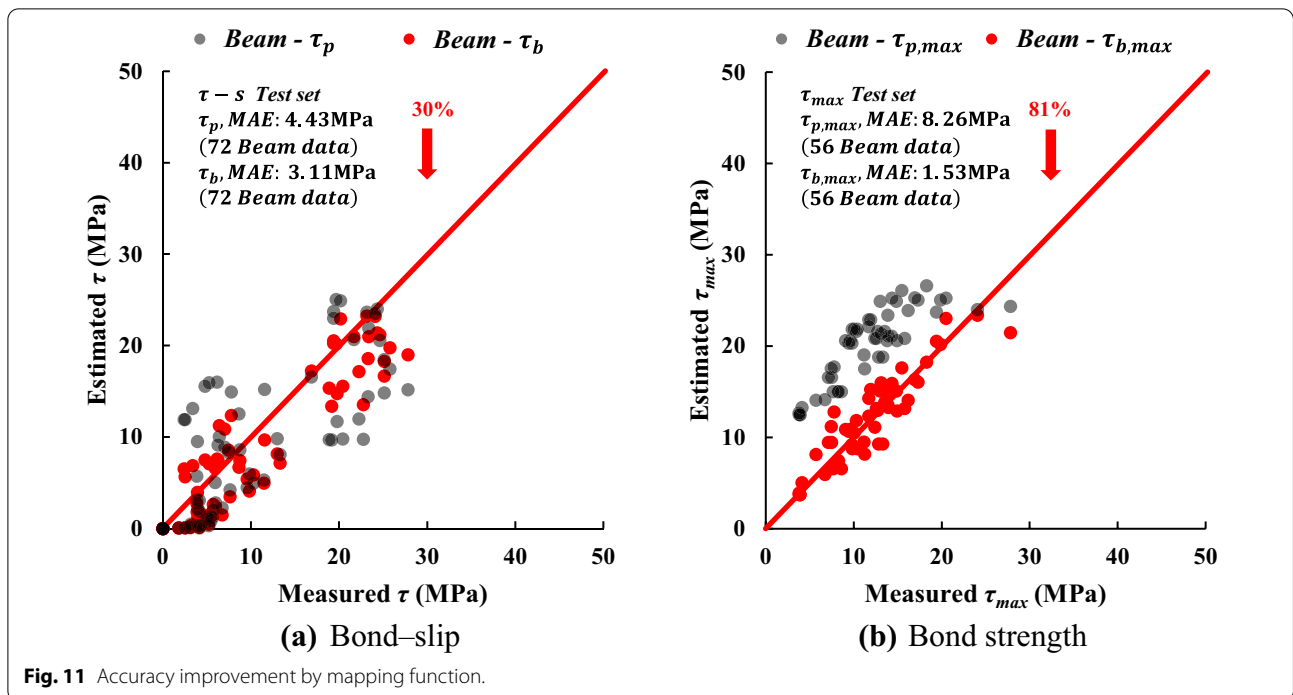
As in Eq. (17), τ_b has a maximum point at the same position ($s = 1$) as τ_p according to the chain rule, and the bond strength of the beam specimens ($\tau_{b,max}$) is

$$\tau_{b,max} = \frac{(A_{st1}/S_{st} + 2.7)f'_c - 16}{210\frac{d_b}{c} + 7\tau_{p,max} - 10} \tau_{p,max}. \quad (18)$$

A safety factor (γ) is introduced to use Eq. (18) as a design equation as below:

$$\gamma \tau_{b,max} = \gamma \frac{(A_{t1}/S_t + 2.7)f'_c - 16}{210\frac{d_b}{c} + 7\tau_{p,max} - 10} \tau_{p,max}. \quad (19)$$





5 Verification

5.1 Accuracy of Proposed Models

Fig. 10a shows the prediction accuracy of the bond-slip models for the pull-out and beam specimens in Eqs. (12) and (16), respectively. One-third of 1785 data points from the pull-out tests and one-third of 217 data points from the beam tests were used for the validation of the proposed models. (i.e., 590 data points from the pull-out tests and 72 data points from the beam tests). In the figure, the black dots indicate the τ of the pull-out specimens predicted using Eq. (12), while the red dots indicate

the τ of the beam specimens predicted using Eq. (16). As shown in the figure, both models predicted τ with high levels of accuracy, and Eqs. (12) and (16) showed MAEs of 2.04 and 3.11 MPa, respectively.

Fig. 10b shows the τ_{max} prediction accuracy of Eqs. (14) and (18) for 101 data points from the pull-out test and 56 data points from the beam test (including additional 44 data points of τ_{max}) except for the τ_{max} used for training. The black dots indicate the τ_{max} of the pull-out specimens predicted using Eq. (14), while the red dots indicate the τ_{max} of the beam specimens predicted using Eq. (18). As

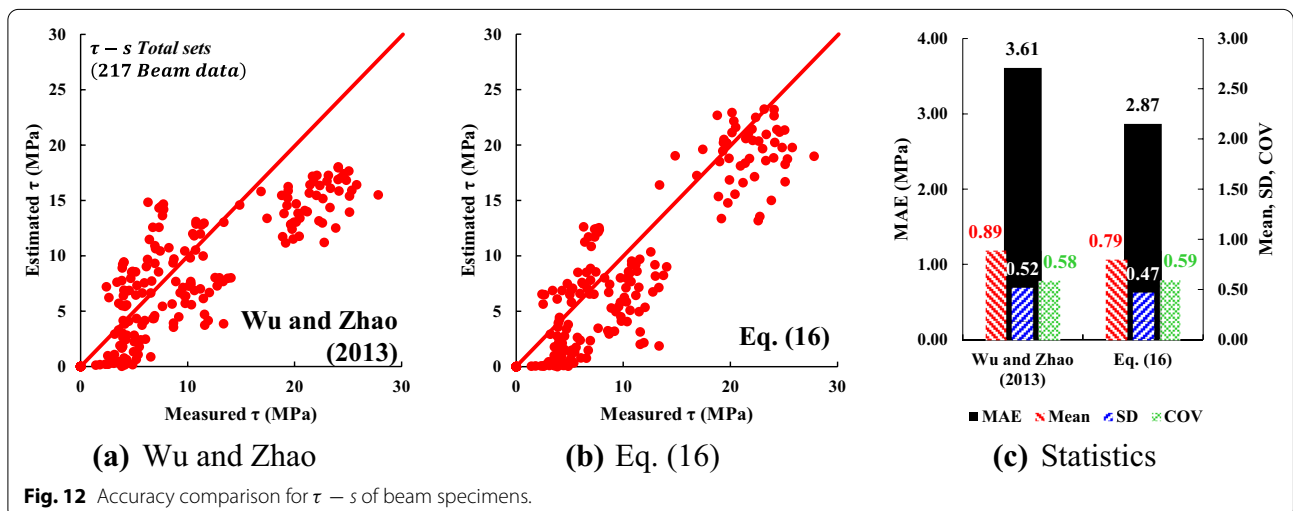
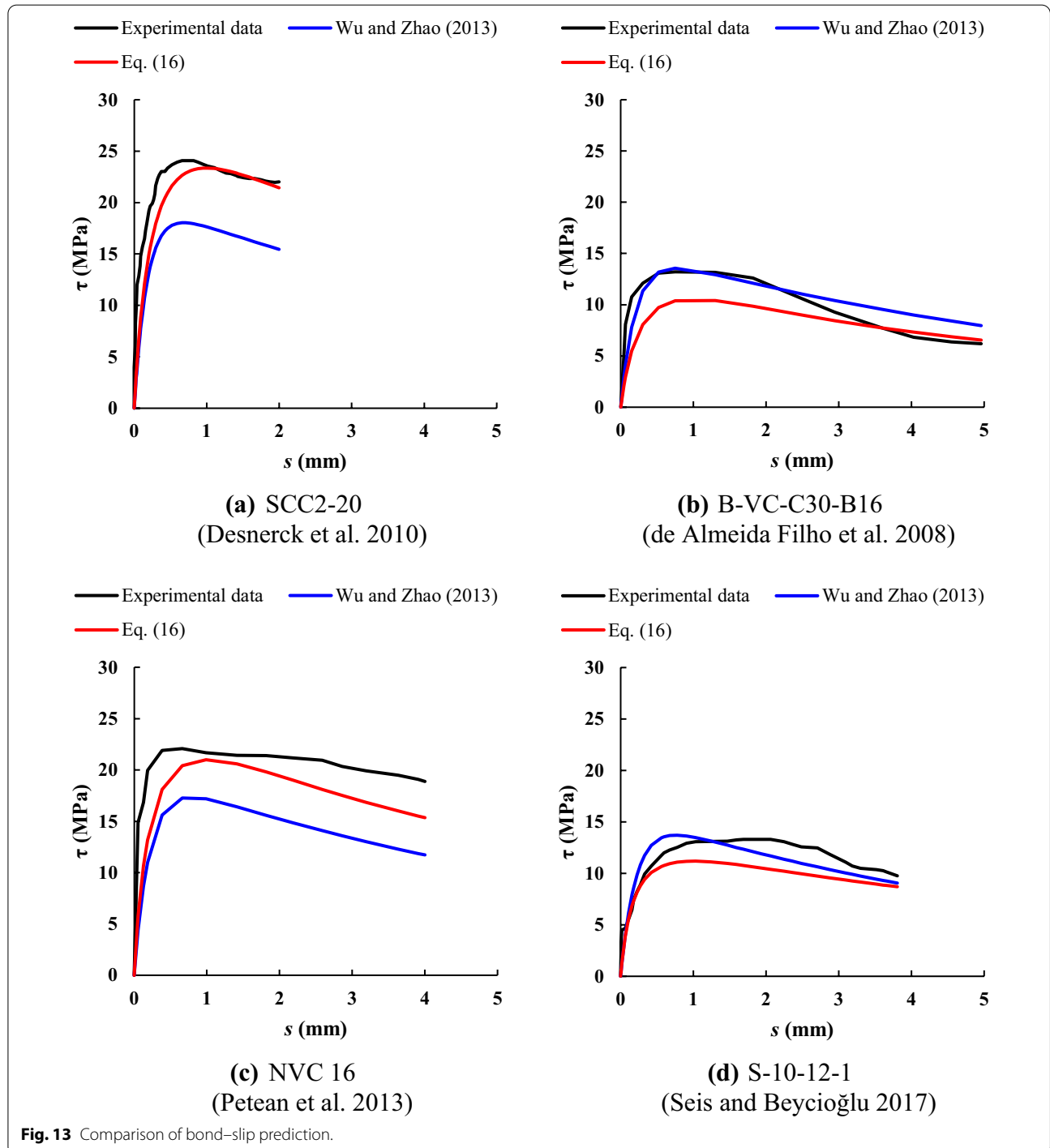


Fig. 12 Accuracy comparison for $\tau - s$ of beam specimens.

shown in the figure, Eqs. (14) and (18) provided prediction results close to the ideal curve and showed MAEs of 2.80 and 1.53 MPa, respectively.

A comparison between the accuracy of Eqs. (12) and (14) and that of Eqs. (16) and (18) for beam specimens reveals the accuracy improvement effect owing to the

mapping function. The black and red dots in Fig. 11a indicate the τ of the beam specimens predicted using Eqs. (12) and (16), respectively. When the τ of the beam specimens was predicted using Eq. (12), the MAE was 4.43 MPa. When the mapping function was used for



prediction, the MAE was 3.11 MPa, reducing the error by approximately 30%.

The black and red dots in Fig. 11b indicate the τ_{max} of the beam specimens predicted using Eqs. (14) and (18), respectively. In general, the measured τ_{max} values of the pull-out specimens are larger than those of the beam specimens. Therefore, Eq. (14), trained using pull-out

data, evaluated the τ_{max} of the beam specimens as very unsafe. As a result, the MAE of Eq. (14) was 8.26 MPa, and the MAE of Eq. (18) was 1.53 MPa, reducing the error by 81%.

In Fig. 12, the τ prediction accuracy of the model proposed by Wu and Zhao (2013) and that of Eq. (16) are compared. The mean, standard deviation (SD), and

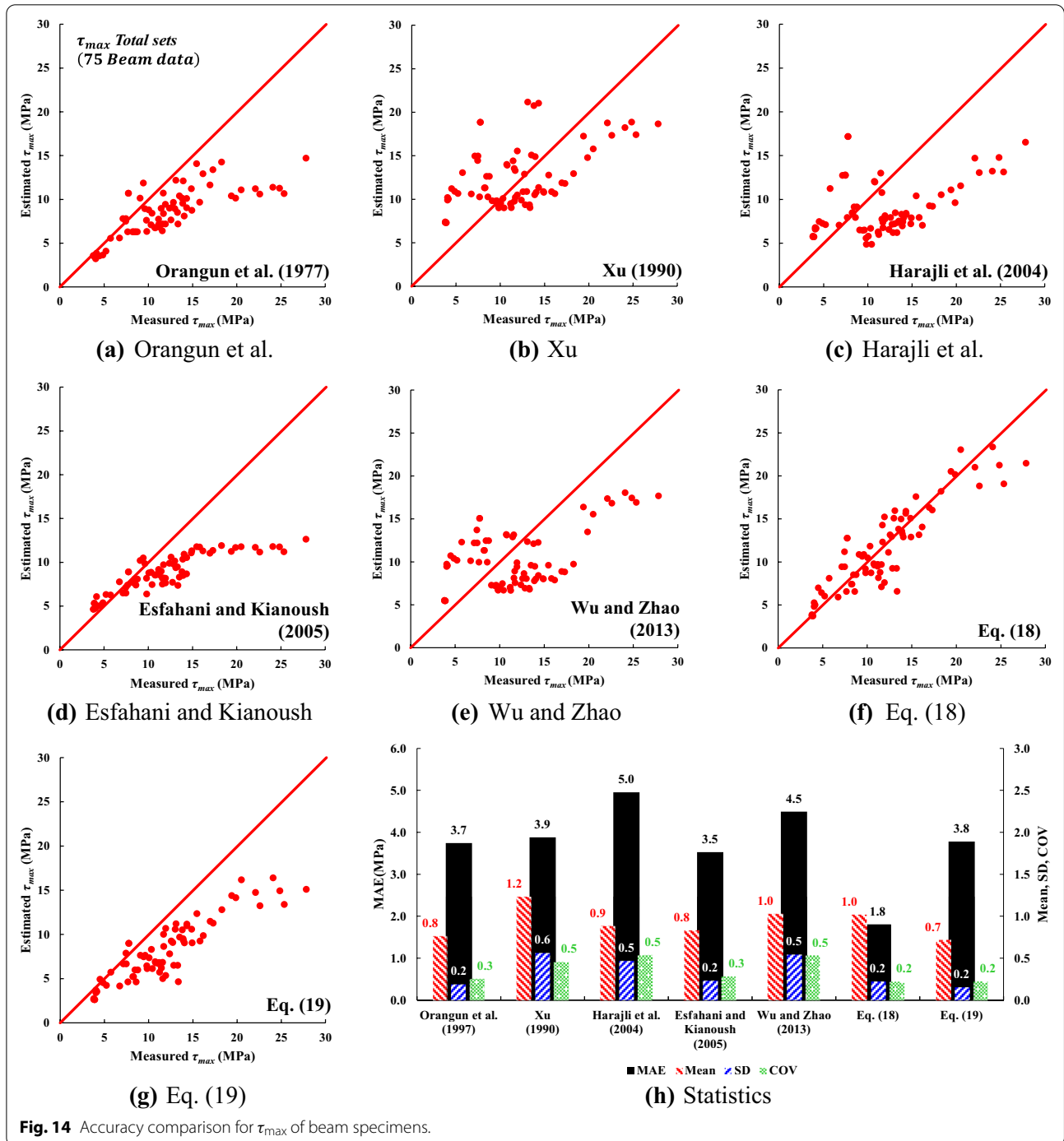


Fig. 14 Accuracy comparison for τ_{max} of beam specimens.

coefficient of variation (COV) are statistical values based on the values which are divided the predicted value into the measured value. The model by Wu and Zhao showed an MAE of 3.6 MPa, while Eq. (16) had an MAE of 2.9 MPa, exhibiting a predicted behavior closer to the ideal curve. The proposed model provides conservative prediction results at the interval with a lower τ than that of Wu and Zhao’s model. Consequently, the mean of those were 0.9 and 0.8, and the SD and COV of the two models were 0.5 and 0.6, respectively.

Fig. 13 compares the $\tau - s$ curve obtained by the model proposed by Wu and Zhao (2013) and Eq. (16) with the beam test data. Both models exhibited excellent accuracy. However, in the case of Fig. 13a, c with a high τ_{max} , the proposed model simulated the $\tau - s$ behavior more closely, whereas, in the case of Fig. 13b, d with low τ_{max} , the model proposed by Wu and Zhao (2013) showed results that were slightly closer to the experimental results. The low accuracy in the high τ region of Wu and Zhao’s model was due to the lack of high-strength specimen data used for modeling. On the other hand, the reason for the low accuracy in the low τ region of the proposed model seemed to be due to the limited model complexity during evolution.

Fig. 14 shows comparison results of τ_{max} obtained from the existing models, Eqs. (18), and (19). In the model proposed by Xu (Xu, 1990), f_t was calculated (ACI committee318, 2019) as

$$f_t = 0.5\sqrt{f'_c} \tag{20}$$

In the model used by Orangun et al. (1977), $f_{yt} = 400$ MPa was applied to specimens for which f_{yt} was not reported. As shown in Table 8, 0.7, which is a value at 0.08 fractile, was applied as a safety factor (γ) in Eq. (19).

Table 8 Relationship between safety factor and fractile

Fractile	γ
0.05	0.65
0.08	0.70
0.10	0.73
0.15	0.79
0.20	0.84
0.25	0.88
0.30	0.91
0.35	0.94
0.40	0.98
0.45	1.01
0.50	1.04

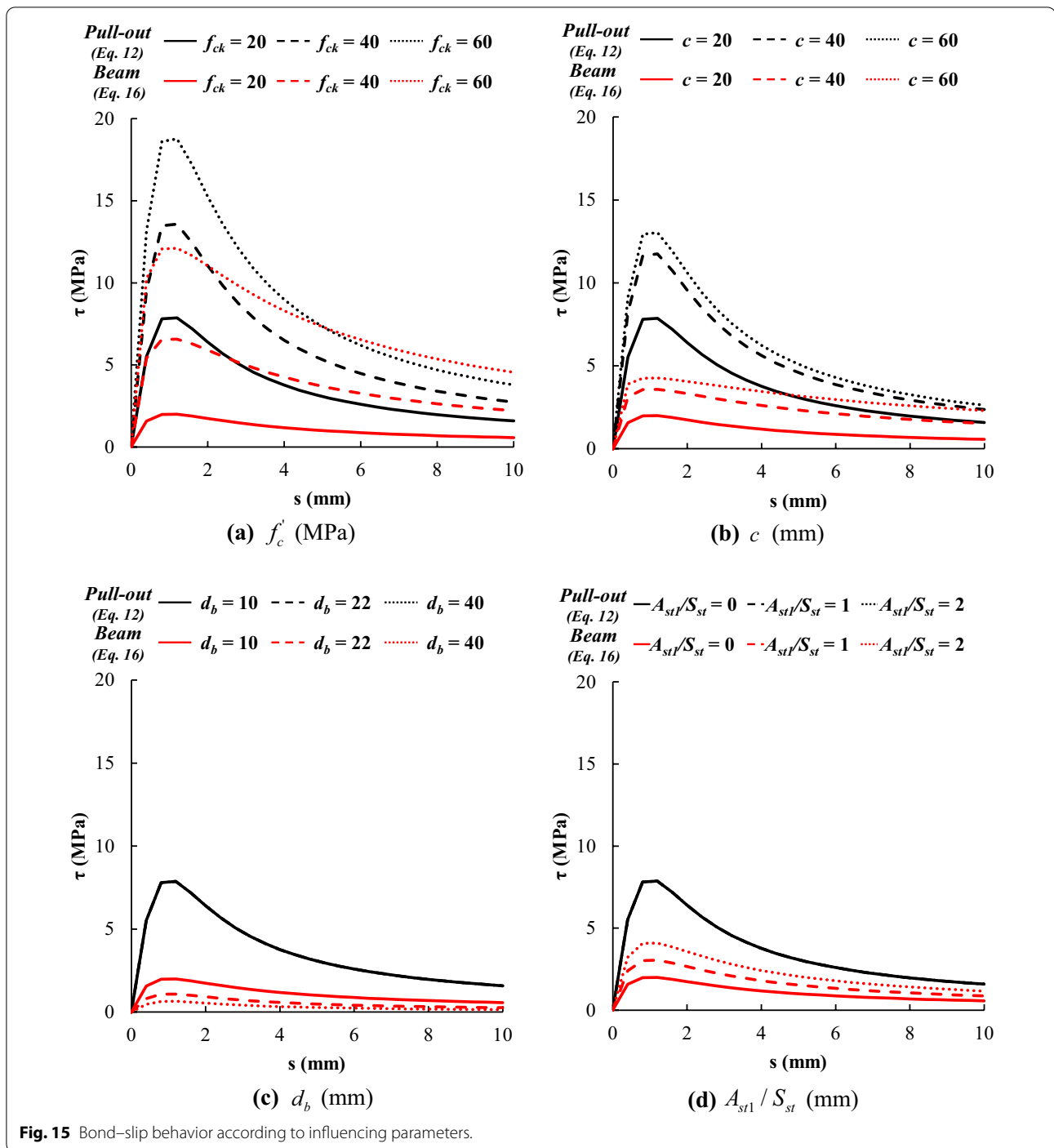
As shown in Fig. 14h, Eq. (18) showed the lowest MAE (1.8 MPa) and a mean of 1.0, and Eq. (19) provided conservative τ_{max} values. Equations (18) and (19) showed the lowest SD and COV, and the models of Esfahani and Kianoush (2005) and Orangun et al. (1977) also showed a low SD and COV. These results indicate that Eq. (18) can predict bond–slip and bond strength close to the measured values and also provide bond strength on the safe side by introducing a safety factor.

5.2 Bond–Slip Behavior of Proposed Models

In this section, Eq. (12) (i.e., the $\tau - s$ model for pull-out specimens) and Eq. (16) (i.e., the $\tau - s$ model for beam specimens), the accuracies of which were verified in Sect. 5.1, were used to analyze the change in $\tau - s$ resulting from the influence of each variable and to compare the difference in the $\tau - s$ behavior between the pull-out and beam specimens. In Fig. 15, the black and red lines indicate the $\tau - s$ behavior of Eqs. (12) and (16), and the values of each feature increase in the order of solid, dashed, and dotted lines. Fig. 15a shows the effect of f'_c . As f'_c increased, the τ values of Eqs. (12) and (16) were found to increase significantly. In addition, the τ_{max} of Eq. (16) was approximately 6–7 MPa lower than that of Eq. (12), and Eq. (16) showed a less sharp decrease in τ at the post-peak stage compared with that of Eq. (12). Fig. 15b shows the effect of c . In both models, τ increased with increasing c . However, the rate of increase in τ gradually decreased as c increased. The effects of d_b and A_{st1}/S_{st} are shown in Fig. 15c, d, respectively. Because the effects of d_b and A_{st1}/S_{st} were not reflected in the pull-out bond–slip curve of Eq. (12), the $\tau - s$ behavior was the same, even when d_b and A_{st1}/S_{st} changed—that is, it is represented by a single curve in the graphs in Fig. 15c, d. However, the effects of d_b and A_{st1}/S_{st} were reflected in Eq. (16). As a result, the τ of Eq. (16) decreased as d_b increased, and the rate of decrease gradually decreased. In addition, the τ of Eq. (16) increased almost linearly with increasing A_{st1}/S_{st} .

6 Conclusions

In this study, a mapping function was developed to simplify estimating $\tau - s$ in RC beams. A total of 255 pull-out specimen data and 75 beam specimen data were collected, and the feature importance and correlation of the two groups were analyzed based on the data. In addition, the $\tau - s$ model for pull-out specimens (base model) and the $\tau - s$ mapping function between the pull-out and beam specimens were derived using GP. The rationality of the proposed model was verified by comparing its accuracy with that of existing models. The mapping function



proposed can be used to estimate the $\tau - s$ of the beam through a relatively simple pull-out test. In addition, if the mapping function is used together with the bond-slip model of pull-out specimens, the $\tau - s$ curve can be derived without experimental data. The following conclusions were drawn from the results of this study.

1. It was found that f'_c had the greatest influence on the τ of the pull-out specimens, and the degree of influence was the highest in f'_c , followed by c , d_b , and $\frac{A_{st1}}{S_{st}}$. When compared with the pull-out specimens, the influence of f'_c was slightly decreased in the beam specimens. In addition, the influence of A_{st1}/S_{st}

increased significantly, and f'_c had the highest degree of influence, followed by $\frac{A_{stl}}{S_{st}}$, c , and d_b .

- While the MAEs for the $\tau - s$ and τ_{max} of the proposed model were 2.04 and 2.80 MPa, respectively, for the pull-out specimens, the MAEs for the $\tau - s$ and τ_{max} of the proposed model were 3.11 and 1.53 MPa, respectively, for the beam specimens. The proposed model exhibited the lowest error when compared with the existing models.
- The proposed model was used to compare the $\tau - s$ behaviors of the two groups. The comparison revealed that the τ_{max} of the beam specimens was lower than that of the pull-out specimens, and the beam specimens exhibited a more gradual decrease in τ at the post-peak stage when compared with the pull-out specimens.

Acknowledgements

This work was supported by the National Research Foundation of Korea (NRF) grant funded by the Korea government (MSIT). (No. 2019R1A2C2086388).

Author contributions

HJ Methodology, data curation, writing—original draft, conceptualization. SJ Data curation, investigation. JHK Validation, investigation. S-HC Validation, visualization. IH Data curation, visualization. KSK Writing—review and editing, funding acquisition. All authors read and approved the final manuscript.

Authors' Information

Hoseong Jeong is a Ph.D. candidate in the department of architectural engineering of University of Seoul. He received B.S. degrees in material science & engineering and architectural engineering and an M.S. degree in architectural engineering from University of Seoul. His research interest focus on machine learning in structural engineering.

Seongwoo Ji is a graduate student in the department of architectural engineering of University of Seoul. His research interest is the bond–slip behavior in reinforced concrete.

Jae Hyun Kim is a Ph.D. candidate in the department of architectural engineering of University of Seoul. He received a B.S. and M.S. in architectural engineering from University of Seoul. His research interest is the analysis of beam–column joints.

Seung-Ho Choi is a postdoctoral researcher in the department of architectural engineering of University of Seoul. He received a B.S., M.S., and Ph.D. in architectural engineering from University of Seoul. His research interest is the analysis of beam–column joints.

Inwook Heo is a Ph.D. candidate in the department of architectural engineering of University of Seoul. He received a B.S. and M.S. in architectural engineering from University of Seoul. His research interest is the fire safety.

Kang Su Kim is a professor in the department of architectural engineering of University of Seoul. He received a B.S., M.S. in architectural engineering from Inha University and a Ph.D. in civil engineering from University of Illinois Urbana-Champaign. His research interest is the structural analysis of prestressed concrete members.

Funding

National Research Foundation of Korea (NRF) grant funded by the Korea government (MSIT). (No. 2019R1A2C2086388).

Availability of data and materials

All data that support the findings of this study are available from the corresponding author upon reasonable request.

Declarations

Competing interests

The authors declare no competing interests.

Author details

¹Department of Architectural Engineering and Smart City Interdisciplinary Major Program, University of Seoul, 163 Seoulsiripdaero, Dongdaemun-gu, Seoul 02504, Republic of Korea. ²Department of Architectural Engineering, University of Seoul, 163 Seoulsiripdaero, Dongdaemun-gu, Seoul 02504, Republic of Korea.

Received: 16 February 2022 Accepted: 21 May 2022

Published online: 20 September 2022

References

- Alharbi, Y. R., Galal, M., Abadel, A. A., & Kohail, M. (2021). Bond behavior between concrete and steel rebars for stressed elements. *Ain Shams Engineering Journal*, 12(2), 1231–1239. <https://doi.org/10.1016/J.ASEJ.2020.10.001>
- Baena, M., Torres, L., Turon, A., & Barris, C. (2009). Experimental study of bond behaviour between concrete and FRP bars using a pull-out test. *Composites Part b: Engineering*, 40(8), 784–797. <https://doi.org/10.1016/J.COMPOSITESB.2009.07.003>
- Breiman, L. (2001). Random forests. *Machine Learning*, 45(1), 5–32. <https://doi.org/10.1023/A:1010933404324>
- Breiman, L., Friedman, J., Stone, C. J., & Olshen, R. A. (1984). *Classification and regression trees*. CRC Press. <https://doi.org/10.2307/2530946>
- Comité Euro-International du Béton. (1993). *CEB-FIP model code 1990: Design code* (1st ed.). Thomas Telford Publishing.
- Darwin, D., McCabe, S. L., Idun, E. K., & Schoenekase, S. P. (1992). Development length criteria: Bars not confined by transverse reinforcement. *ACI Structural Journal*. <https://doi.org/10.14359/4158>
- de Almeida Filho, F. M., El Debs, M. K., & El Debs, A. L. H. C. (2008). Bond-slip behavior of self-compacting concrete and vibrated concrete using pull-out and beam tests. *Materials and Structures*, 41(6), 1073–1089. <https://doi.org/10.1617/s11527-007-9307-0>
- Desnerck, P., De Schutter, G., & Taerwe, L. (2010). Bond behaviour of reinforcing bars in self-compacting concrete: Experimental determination by using beam tests. *Materials and Structures*, 43(51), 53–62. <https://doi.org/10.1617/s11527-010-9596-6>
- Engstrom, B., Magnusson, J., & Huang, Z. (1998). Pull-out bond behavior of ribbed bars in normal and high-strength concrete with various confinements. *ACI Symposium Publication*, 180, 215–242. <https://doi.org/10.14359/5879>
- Esfahani, M. R., & Kianoush, M. R. (2005). Development/splice length of reinforcing bars. *ACI Structural Journal*, 102(1), 22.
- Granitto, P. M., Furlanello, C., Biasoli, F., & Gasperi, F. (2006). Recursive feature elimination with random forest for PTR-MS analysis of agroindustrial products. *Chemometrics and Intelligent Laboratory Systems*, 83(2), 83–90. <https://doi.org/10.1016/j.chemolab.2006.01.007>
- Harajli, M. H., Hout, M., & Jalkh, W. (1995). Local bond stress-slip behavior of reinforcing bars embedded in plain and fiber concrete. *ACI Materials Journal*, 92(4), 343–353. <https://doi.org/10.14359/999>
- Hou, L., Xu, R., Zang, Y., Ouyang, F., Chen, D., & Zhong, L. (2020). Bond behavior between reinforcement and ultra-high toughness cementitious composite in flexural members. *Engineering Structures*, 210, 110357. <https://doi.org/10.1016/J.ENGSTRUCT.2020.110357>
- Ichinose, T., Kanayama, Y., Inoue, Y., & Bolander, J. E. (2004). Size effect on bond strength of deformed bars. *Construction and Building Materials*, 18(7), 549–558. <https://doi.org/10.1016/j.conbuildmat.2004.03.014>
- Kim, S.-W., Yun, H.-D., Park, W.-S., & Jang, Y.-I. (2015). Bond strength prediction for deformed steel rebar embedded in recycled coarse aggregate concrete. *Materials & Design*, 83, 257–269. <https://doi.org/10.1016/j.matdes.2015.06.008>
- Koza, J. (1994). Genetic programming as a means for programming computers by natural selection. *Statistics and Computing*. <https://doi.org/10.1007/BF00175355>

- Kuhn, M., & Johnson, K. (2019). *Feature engineering and selection: A practical approach for predictive models* (1st ed.). CRC Press.
- Lee, J. Y., Yi, C. K., Cheong, Y. G., & Kim, B. I. (2012). Bond stress–slip behaviour of two common GFRP rebar types with pullout failure. *Magazine of Concrete Research*, 64(7), 575–591. <https://doi.org/10.1680/mac.11.00050>
- Levenberg, K. (1944). A method for the solution of certain non-linear problems in least squares. *Quarterly of Applied Mathematics*, 2(2), 164–168. <https://doi.org/10.1090/qam/10666>
- Lin, H., & Zhao, Y. (2016). Effects of confinements on the bond strength between concrete and corroded steel bars. *Construction and Building Materials*, 118, 127–138. <https://doi.org/10.1016/J.CONBUILDMAT.2016.05.040>
- Liu, X., Liu, Y., Wu, T., & Wei, H. (2020). Bond-slip properties between lightweight aggregate concrete and rebar. *Construction and Building Materials*, 255, 119355. <https://doi.org/10.1016/J.CONBUILDMAT.2020.119355>
- Ma, Y., Guo, Z., Wang, L., & Zhang, J. (2017). Experimental investigation of corrosion effect on bond behavior between reinforcing bar and concrete. *Construction and Building Materials*, 152, 240–249. <https://doi.org/10.1016/J.CONBUILDMAT.2017.06.169>
- Marquardt, D. W. (1963). An algorithm for least-squares estimation of nonlinear parameters. *Journal of the Society for Industrial and Applied Mathematics*, 11(2), 431–441. <https://doi.org/10.1137/0111030>
- Martin, H. (1973). On the interrelation among surface roughness, bond and bar stiffness in the reinforcement subject to short-term loading. *Deutscher Ausschuss Stahlbeton*, 228, 1–50.
- Mazumder, M. H., & Gilbert, R. I. (2019). Finite element modelling of bond–slip at anchorages of reinforced concrete members subjected to bending. *SN Applied Sciences*, 1(11), 1332. <https://doi.org/10.1007/s42452-019-1368-5>
- Melo, J., Rossetto, T., & Varum, H. (2015). Experimental study of bond–slip in RC structural elements with plain bars. *Materials and Structures*, 48(8), 2367–2381. <https://doi.org/10.1617/s11527-014-0320-9>
- Miller, B. L., & Goldberg, D. E. (1995). Genetic algorithms, tournament selection, and the effects of noise. *Complex Systems*, 9(3), 193–212.
- Mo, Y. L., & Chan, J. (1996). Bond and slip of plain rebars in concrete. *Journal of Materials in Civil Engineering*, 8(4), 208–211. [https://doi.org/10.1061/\(ASCE\)0899-1561\(1996\)8:4\(208\)](https://doi.org/10.1061/(ASCE)0899-1561(1996)8:4(208))
- Orangun, C. O., Jirsa, J. O., & Breen, J. E. (1977). A reevaluation of test data on development length and splices. *ACI Journal Proceedings*, 74(3), 114–122. <https://doi.org/10.14359/10993>
- Petean, A.-I., Sabau, M., & Onet, T. (2013). Bond-slip behavior of self compacting concrete. *Buletinul Institutului Politehnic Din Lasii. Sectia Constructii, Arhitectura*, 59(1), 139.
- Prince, M. J. R., & Singh, B. (2013). Bond behaviour of deformed steel bars embedded in recycled aggregate concrete. *Construction and Building Materials*, 49, 852–862. <https://doi.org/10.1016/J.CONBUILDMAT.2013.08.031>
- Rehm, G. (1961). On the fundamentals of steel-concrete bond. *Deutscher Ausschuss Für Stahlbeton*, 138, 1–59.
- Robert, G. M., & David, W. (1961). Investigation of bond in beam and pull-out specimens with high-yield -strength deformed bars. *ACI Journal Proceedings*. <https://doi.org/10.14359/8058>
- Rousseeuw, P. J. (1987). Silhouettes: A graphical aid to the interpretation and validation of cluster analysis. *Journal of Computational and Applied Mathematics*, 20, 53–65. [https://doi.org/10.1016/0377-0427\(87\)90125-7](https://doi.org/10.1016/0377-0427(87)90125-7)
- Seis, M., & Beycioğlu, A. (2017). Bond performance of basalt fiber-reinforced polymer bars in conventional Portland cement concrete: A relative comparison with steel rebar using the hinged beam approach. *Science and Engineering of Composite Materials*, 24(6), 909–918. <https://doi.org/10.1515/secm-2015-0210>
- Solyom, S., & Balázs, G. L. (2020). Bond of FRP bars with different surface characteristics. *Construction and Building Materials*, 264, 119839. <https://doi.org/10.1016/j.conbuildmat.2020.119839>
- Song, X., Wu, Y., Gu, X., & Chen, C. (2015). Bond behaviour of reinforcing steel bars in early age concrete. *Construction and Building Materials*, 94, 209–217. <https://doi.org/10.1016/J.CONBUILDMAT.2015.06.060>
- Soroushian, P., & Choi, K.-B. (1989). Local bond of deformed bars with different diameters in confined concrete. *ACI Structural Journal*, 86(2), 217–222.
- Soroushian, P., Choi, K.-B., Park, G.-H., & Aslani, F. (1991). Bond of deformed bars to concrete: Effects of confinement and strength of concrete. *ACI Materials Journal*, 88(3), 227–232.
- Sturm, A. B., & Visintin, P. (2019). Local bond slip behavior of steel reinforcing bars embedded in ultra high performance fibre reinforced concrete. *Structural Concrete*, 20(1), 108–122. <https://doi.org/10.1002/suco.201700149>
- Teppers, R. (1979). Cracking of concrete cover along anchored deformed reinforcing bars. *Magazine of Concrete Research*, 31(106), 3–12. <https://doi.org/10.1680/mac.1979.31.106.3>
- Timoshenko, S. (2002). *Strength of materials: Part 2, advanced theory and problems* (3rd ed.). CBS Publishers & Distributors Pvt. Ltd.
- Walker, P. R., Batayneh, M. K., & Regan, P. E. (1997). Bond strength tests on deformed reinforcement in normal weight concrete. *Materials and Structures*, 30(7), 424–429.
- Wu, Y.-F., & Zhao, X.-M. (2013). Unified bond stress–slip model for reinforced concrete. *Journal of Structural Engineering*, 139(11), 1951–1962. [https://doi.org/10.1061/\(ASCE\)ST.1943-541X.0000747](https://doi.org/10.1061/(ASCE)ST.1943-541X.0000747)
- Wu, Z., Zhang, X., Ma, Z., Li, X., & Yu, R. C. (2021). Bond behavior of deformed bars in self-compacting lightweight aggregate concrete at early ages. *Journal of Materials in Civil Engineering*, 33(2), 04020460. [https://doi.org/10.1061/\(ASCE\)MT.1943-5533.0003573](https://doi.org/10.1061/(ASCE)MT.1943-5533.0003573)
- Xu, R., & Wunsch, D. C. (2008). *Clustering* (Vol. 10). Wiley. <https://doi.org/10.1002/9780470382776>
- Yalciner, H., Eren, O., & Sensoy, S. (2012). An experimental study on the bond strength between reinforcement bars and concrete as a function of concrete cover, strength and corrosion level. *Cement and Concrete Research*, 42(5), 643–655. <https://doi.org/10.1016/J.CEMCONRES.2012.01.003>
- Yerlici, V. A., & Ozturan, T. (2000). Factors affecting anchorage bond strength in high-performance concrete. *ACI Structural Journal*, 97(3), 499–507.
- Zhou, H., Lu, J., Xu, X., Dong, B., & Xing, F. (2015). Effects of stirrup corrosion on bond–slip performance of reinforcing steel in concrete: An experimental study. *Construction and Building Materials*, 93, 257–266. <https://doi.org/10.1016/J.CONBUILDMAT.2015.05.122>
- ACI committee 318. (2019). *Building code requirements for structural concrete (ACI 318–19) and commentary (ACI 318R–19)*. Farmington Hills: American Concrete Institute (ACI).
- Campione, G., Cucchiara, C., La Mendola, L., & Papia, M. (2004). Experimental investigation on local bond-slip behaviour in lightweight fiber reinforced concrete under cyclic actions. In *13th World Conference on Earthquake Engineering*. Vancouver.
- Deng, H., Runger, G., & Tuv, E. (2011). Bias of importance measures for multi-valued attributes and solutions BT-Artificial Neural Networks and Machine Learning—ICANN 2011. In T. Honkela, W. Duch, M. Girolami, & S. Kaski (Eds.), (pp. 293–300). Springer Berlin Heidelberg.
- Ding, C., & He, X. (2004). K-means clustering via principal component analysis. *Proceedings of the twenty-first international conference on Machine learning*, 225–232. <https://doi.org/10.1145/1015330.1015408>
- Eligehausen, R., Popov, E. P., & Bertero, V. V. (1982). *Local bond stress-slip relationships of deformed bars under generalized excitations*.
- Kemp, E. L., & Wilhelm, W. J. (1979). Investigation of the parameters influencing bond cracking. In *ACI Journal proceedings* (Vol. 76, pp. 47–72).
- Lutz, L. A., & Gergely, P. (1967). Mechanics of bond and slip of deformed bars in concrete. In *ACI Journal Proceedings* (Vol. 64, pp. 711–721).
- Mirza, S. M., & Houde, J. (1979). Study of bond stress–slip relationships in reinforced concrete. In *ACI Journal Proceedings* (Vol. 76, pp. 19–46).
- Nilson, A. H. (1968). Nonlinear analysis of reinforced concrete by the finite element method. In *ACI Journal Proceedings* (Vol. 65, pp. 757–766).
- Tastani, S. P., & Pantazopoulou, S. J. (2002). Experimental evaluation of the direct tension-pullout bond test. In *Bond in Concrete—from research to standards*. Budapest.
- Xu, Y. (1990). Experimental study of anchorage properties for deformed bars in concrete. Beijing, Tsinghua.

Publisher's Note

Springer Nature remains neutral with regard to jurisdictional claims in published maps and institutional affiliations.